International Journal of Engineering Trends and Technology
ISSN: 2231 – 5381 / https://doi.org/10.14445/22315381/IJETT-V70I11P237
Volume 70 Issue 11, 353-363, November 2022

Original Article

Asial CNN: Assorted Scale Integrated Alternate Link Model Convolutional Neural Network for Lung Nodule Detection

S. Parveen Banu[1], M. Syed Mohamed[2]

[1,2]*Department of IT, Sri Ram Nallamani Yadava College of Arts and Science, Manonmaniam Sundaranar University, Tamilnadu, India*

[1]*Corresponding Author : parveenbanuresearch1@gmail.com*

Received: 09 June 2022 Revised: 02 September 2022 Accepted: 26 September 2022 Published: 26 November 2022

Abstract *- Early-stage lung cancer is characterized mostly by the presence of lung nodules, a common symptom of the illness. It is critical to have an imaging system that can identify lung nodules automatically and accurately. In addition to reducing the burden on radiologists, automatic detection minimizes the incidence of misdiagnosis. Despite their outstanding performance, convolutional neural networks (CNNs) need certain anchor parameters, such as the size, number, and aspect ratio of anchors, and have limited resilience when dealing with a wide range of lung nodule sizes. The ASIAL CNN (assorted scale integrated alternative link model convolutional neural network) is a solution to these issues by automatically predicting nodule location, radius, and offset without the need for any custom nodule/anchor parameters to be designed. Three-level parallelism in the SIAL CNN is achieved by varying the convolution kernel size for the inputs with multi-scale properties. Here, the precession layer's output is coupled to its succession stage input and the succession stage input of the following layer. Binary classifications like benign and malignant lung nodules may be processed using this method, as shown by the results it achieves. It was all done using a graphics processing unit (GPU). The LIDC-IDRI dataset indicated that our proposed ASIAL CNN architecture outperforms current approaches for lung nodule identification with an average accuracy of 92.45%.*

Keywords *- Lung cancer, lung nodule, assorted scale integrated alternate link model convolutional neural network.*

1. Introduction

(In recent years, the number of people diagnosed with lung cancer has increased alarmingly. Detecting lung nodules promptly and properly is critical to the treatment of lung cancer since lung nodules are an early symptom of the disease. Particular clinical and scientific relevance rests on the discovery of lung nodules. Round or irregularly shaped lesions on the lungs are known as pulmonary nodules (PN). CT imaging of the lungs shows it as a thick shadow with obvious or ambiguous borders. There are three types of nodules: solid, partial, and ground-glass density, which may all be categorized based on the tumor's characteristics. In contrast to a solid nodule, a ground glass density nodule has a low grey value and may be distinguished from the surrounding tissues by its low grey value. Soft tissue with different densities may be found inside some solid nodules.

Radiologists can detect whether there are any lung nodules by manually reviewing a large number of images. Some patients require as many as hundreds of lung CT images to acquire an accurate diagnosis. Misdiagnosis is more likely when physicians are fatigued, and an inefficient and lengthy procedure hampers their results. A computer-aided detection strategy has been proposed by researchers to prevent this from happening as much as feasible. These two tasks are frequently done individually in CAD, although they may be combined. The use of second-stage screening prevents false positives for these potentially harmful lesions. Various approaches, including morphology and form curvature, may be used to identify potential frames. A popular technique for reducing false alarms combines location, size, shape, and density with texture, gradient cues, and information about upper and lower individuals. However, even though the standard computer-aided inspection method obtained good results, there are still two obvious flaws: A major problem with the system's overall efficiency: Secondly, the detection hypothesis and the real circumstance are vastly different, resulting in an overall decrease in detection accuracy. Due to the vast quantity of data and complete feature extraction, deep learning provides strong classification and recognition performance. According to a recent study, deep learning is now being used to identify lung nodules. It is one of the most widely used deep learning models and is particularly useful for image categorization. It is a well-known neural network-based target identification technique. In order to fully detect the target, we include the CNN scales here. It is possible to get reliable test results since the detection procedure is end-to-end and done entirely on GPU. It has advantages over traditional approaches in terms of data processing, network

resilience, and minimizing over-fitting risk; second, it has advantages in terms of the pooling operation, which further reduces computation and significantly improves data processing efficiency; and finally, it can extract extremely abstract feature maps depending on the depth of the feature extraction network. Scale depth is critical in the proposed structure. These are some of the findings from this research.:

- In this paper, we provide an abnormal lung nodule prediction approach based on deep learning-based Assorted SIAL CNN architecture.
- This technique is compared against state of art using measures from real-world datasets and shown to be superior.

The following summary of the paper's remaining sections: Section two summarises the related works. The issue statement is explained in Section 3. Section 4 explains the use of deep learning to discover abnormal lung nodules. Section 5 presents the findings. The paper comes to an end in Section 6.

2. Related Works

There are many existing methods for classifying lung nodules, some of which are shown below. These lung nodules may be detected using a Faster R-CNN method proposed in [1]. Using a training set of lung nodules, an R-CNN system can quickly and accurately identify lung nodules. Network structure and detection accuracies may be improved through parameter tuning in principle. Deep learning-based lung nodule screening and analysis methodologies are examined in [2] to understand better the present performance, constraints, and trends in the study of lung nodules via an evaluation of their clinical applications. [3] proposes three-dimensional squeeze-and-excite attention modules (three-dimensional squeeze-and-excite). A method of dense feature extraction and integrated multi-dilated context learning was developed [4] using dilated convolutions run at different rates. Using k-mean clustering and morphological operators, lung ROIs may be retrieved from CT scans instead of whole images or nodular patches. These ROIs might be used to create a nodule segmentation architecture that can handle various types of lung nodules. Filtering and noise reduction were used in the pre-processing stage [5]. It is also possible to identify lung nodules using the adaptive thresholding approach (OTSU) and semantic segmentation. The features of 13 nodules were extracted using the principal components analysis method. In addition, four top features are picked based on the algorithm's classification performance. During the classification phase of the experiment, nine different classifiers are utilized. The author of [6] investigated the diagnostic utility of 64-slice spiral CT and MRI high-resolution images based on deep convolutional neural networks for lung cancer detection (CNN). The random domain adversarial learning (RDAL) approach developed in [7] aims to back-propagate effective gradient signals and gradually reduce the gap across diverse domains. The ATM may be used in combination with nodule detection models to train the system from start to finish using a differentiable Fast Fourier Transform (FFT) and inverse FFT. The author created and assessed a set of radiomic characteristics dubbed "morphological dynamics features" to detect pulmonary nodules in [8], which were based on dynamic patterns of morphological change and lacked accurate lesion segmentation in the investigation. The author presented a unique deep learning approach in [9] to improve the classification accuracy of lung nodules on CT images. They present the CNN-5CL approach, which uses an 11-layer CNN (5 convolutional layers) for automated feature extraction and categorization. The regularized V-net (RFR V-Net) is recommended in [10] for diagnosing lung cancer nodules with fewer false positives. (FP). In the V-Net model, the convolution and deconvolution layers of the encoder block are receptive and regularized. A novel nodule classification network dubbed nodule classification network combines SqueezeNet and ResNet.In [11], to minimize picture noise, the author used the Grey Wolf Optimization method with a weighted filter and watershed transformation and dilation procedures to segment images. For early lung nodule identification and localization using CT images, [12] provides a methodology that incorporates RF optimization and analysis of the feature groups. In [13], a successful CAD system for detecting lung tumours is discussed. Nodule categorization, segmentation, and early processing are all part of this system. In their study of lung diseases, accurate segmentation of lung images is essential to diagnosing lung cancer. According to [14], a Gabor filter (GF) and an adaptive morphology-based operation have been suggested for accurate lung nodule classification. The 2-Pathway Morphology-based Convolutional Neural Network (2PMorphCNN), a new framework with two trainable pathways, can capture lung nodules' textural and morphological aspects. The ProCAN network, introduced in [15], makes it simpler to classify lung nodules. Using this technique, the issue is attacked from three different sides. First and foremost, they help the Non-Local network by focusing on a single channel. They use curriculum learning concepts for the second part, starting with easier situations and working their way up to more complex ones. Third, when the difficulty of the categorization job increases throughout Curriculum learning, their model grows in size to better handle the current challenge. "3D-CNN," "transferable CNN," "dense convolutional binary tree network," "gated dilated network," and "mask area CNN" are only a few of the advanced convolutional neural networks (CNNs) that the author used in [16]. For the detection and classification of GGO nodules, the author of [17] devised a two-stage 3D architecture. Pulmonary parenchyma was retrieved from the lung using the 3D U-Net first. 3D medical images inspired the development of RCNNs (mask region-based convolutional neural networks). The 3D model was used to find and classify GGO nodules and lesions (benign or malignant). There were equal numbers of benign and malignant lesions, which was achieved using the class-balanced loss function. As the last step toward enhancing detection precision, they used a brand new false-positive elimination technique known as feature-based weighted clustering (FWC). The author suggests solid, semi-solid, and ground glass object texture

classifications in [18] for the characterization of lung nodules. Gray-level co-occurrence matrix and Gabor filters are used to extract features, and the performance is tested on the LNDb dataset. According to [19], an effective technique for deep learning for efficient usage of the completely linked SqueezeNet virtualization with lung pixels was considered through all the extraction of rigorous prediction, which included a beneficial or detrimental characteristic. Dual-energy CT (DECT) is useful in distinguishing between thyroid cancer-related pulmonary metastases and noncancerous lung nodules [20]. They present a unique technique to predict the malignancy of nodules that can examine the tumour's form and size and its density and structure, utilizing a global and local feature extractor, respectively, in [21].In [22], genetic datas were applied to diagnose the malignancy through particle swarm optimization and support vector machine algorithm. However, they used only 29 genetic datas, which is insufficient to determine its efficiency. As per [23], the toboggan algorithm was introduced to segment the lung lobes. Here, the classification was done on normal and diseased lungs but not on malignancy and benign tumors. In [24], three segmentation methods were proposed. Better segmentation was achieved, but the classification was not done.

Table 1. Comparative analysis

Reference	Algorithm	Advantage	Disadvantage
[1]	R-CNN	High accuracy	High overfitting
[2]	Deep learning	Survey knowledge	-
[3]	SCPM-Net	High accuracy	More training time
[4]	efficient U-Net	Less fitting error	Low accuracy
[5]	semantic segmentation	Low testing time	High training time
[6]	Deep CNN	Low testing time	High training time
[7]	AFA	Low testing time	Need more data
[8]	radiomics approach	Low testing time	High-ground truth variation
[9]	CNN	The parameter analysis is simple	Need more data to train
[10]	VNET	User friendly	Need more data to train
[11]	CNN-GWO	High accuracy	Hardware dependence
[12]	Random forest	User friendly	Low accuracy
[13]	Review	-	-
[14]	CNN	High accuracy	High testing time
[15]	ProCAN	High accuracy	Class imbalance
[16]	Review	-	-
[17]	3DNN	High accuracy	Expensive hardware support needed
[18]	ray-level co-occurrence matrix, Gabor filters, and local binary pattern	High accuracy	expensive
[19]	SqueezeNet-Fc	High accuracy	Hard to train
[20]	Parametric method	nil	Mathematical error
[21]	deep local–global networks	Low testing time	expensive
[22]	Machine learning	Survey knowledge	Less dataset
[23]	Toboggan algorithm	High accuracy	No deep classification done
[24]	Adaptive thresholding, Active contour model, Fuzzy C-Means clustering	Improved DSC and Hausdroff distance	No classification done

Hence in this paper, to overcome the existing issues as depicted in table 1, we provide an abnormal lung nodule prediction approach based on deep learning based on Assorted SIAL CNN architecture. The following is a summary of the paper's remaining sections: Section two explains the use of deep learning to discover abnormal lung nodules. Section 3 presents the findings. The paper comes to an end in Section 4.

3. Problem Statement

Survival times for people with lung cancer have been largely lowered because of late diagnosis and a lack of symptoms. Compared to other imaging modalities, CT provides better resolution, quicker acquisition, and lower cost than other imaging techniques. If the nodule is less than 3 millimetres across, CT can detect it. This condition makes preventing the illness from progressing to an advanced stage easier. Nevertheless, in present practice, radiologists review hundreds of thin-section CT pictures produced by each patient and use axial mode to analyze each image. The radiologists tasked with deciphering the massive amounts of data generated by a single CT scan may soon succumb to information overload due to the scan's massive data output.

Consequently, malignancy may be missed if tiny or non-solid nodules are not detected. It is difficult to properly model lung nodules if the nodule diameter is tiny, the slices are thick, the noise is high, the image resolution is poor, and the density of the nodule varies. Interreader variability is the difference between two or more people's interpretations of the same event, as described by their observations. Within-reader variability may be characterized as a disagreement in observations made by a single person, leading to various interpretations of the same event across time. Identification

of nodules is inherently subjective, as shown by the inter- and intra-reader variability even among seasoned radiologists. A large percentage of nodules may go unnoticed on the first scan and only be discovered on subsequent scans in hindsight. A lung nodule may be more effectively treated and more likely to survive if it is discovered early. For this, the radiologist uses a computer-aided diagnostic (CAD) system to assist find nodules by flagging questionable spots. Radiologists use CAD systems as a smart tool that expresses a second viewpoint. As a result, CAD for identifying nodules is becoming increasingly popular. Computer-aided diagnosis (CAD) tools help radiologists better understand medical pictures. According to studies, radiologists may enhance their detection accuracy using CAD systems, reducing the number of nodules missed owing to tiredness and enhancing inter and intra-reader consistency. As an additional benefit, it may assist in minimizing the number of biopsies necessary. An automated computerized system for detecting lung nodules on CT images will be evaluated in this research to see whether it may assist in identifying lung nodules that could otherwise go unnoticed during visual interpretation.

4. Proposed Work

Pulmonary nodules are described as round opacities, well (solid) or poorly defined (part solid, non-solid), measuring 3-30mm in diameter. An automatic CAD system for lung nodule categorization utilizing Assorted SIAL CNNs from CT images is the primary goal of our proposed study. One of the most critical steps in identifying lung nodules is the categorization of the nodule and non-nodule patterns in CT. This aids in the early detection of the condition, which lowers the death rate.

4.1. Dataset

LIDC-IDRI is a worldwide public database that provides training data. A total of 1,018 patients were included in the data set, which was compiled in partnership with seven academic institutions and eight imaging firms. The patient's medical records include CT scans, on which four board-certified radiologists meticulously identified the lesion area using two distinct techniques. Each CT scan was evaluated by four radiologists blindly, who identified which lesions belonged to which of three distinct kinds. In the second step, each radiologist independently verified the other three experts' anonymous markings to offer a comprehensive result. The overall approach aims to enable each radiologist to detect as many full non-nodules as feasible in each CT picture without imposing uniformity. A total of 3,042 nodules considered big by at least one radiologist are included in the data utilized in this article. They may be categorized into three groups: the single lung nodule, the vascular nodule, and the lung wall adhesion nodule.

4.1.1. Data Source

https://wiki.cancerimagingarchive.net/display/Public/LIDCIDRI#:~:text=The%20Lung%20Image%20Database%20Consortium,with%20marked%2Dup%20annotated%20lesions.

4.2. Network Training

The training pace was substantially enhanced before beginning the procedure, which trains a weighted network. As soon as the network model parameters have been established, transmit the proposed region output to the Assorted SIAL CNN for further classification training. The Assorted SIAL CNN parameters learned in the first step are utilized to fine-tune the classifier. For the second round of training, the Assorted SIAL CNN network receives recommendations from the output area. This approach is repeated to guide the network toward convergence.

Multi-task loss functions are described in Equation 1 of the Assorted SIAL CNN model.

$$K(\{q_j\},\{s_j\}) = \frac{1}{M_{cls}}\sum K_{cls}(q_j, q_j^*) + v\frac{1}{M_{reg}}\sum jq_j^* K_{reg}(s_j, s_j^*) \quad (1)$$

Target bounding box category values are predicted as q_j and s_jWhile the actual values are q_j^* and s_j^*; the normalization parameters of classification and regression items areM_{cls} and M_{reg}, respectively; the loss of classification items and the loss of regression items are K_{cls} and K_{reg}, respectively; and the balance weight is w. The classification loss function K_{cls} is represented mathematically in Equation 2.

$$K_{cls}(q_j, q_j^*) = -\log\left(q_j q_j^* + (1-q_j^*)(1-q_j)\right) \quad (2)$$

The regression loss function's expression K_{reg} is illustrated in Equation 3.

$$K_{reg}(s_j, s_j^*) = T(s_j - s_j^*) \quad (3)$$

In Equation 4, T is the robust, smooth K_1 loss.

$$\text{smooth}_{K_1}(s_j, s_j^*) = \begin{cases} 0.5(s-s^*) \text{ if} |s-s^*| < 1 \\ |s-s^*| - 0.5, \text{otherwise} \end{cases} \quad (4)$$

4.3. Classification

It is a deep learning algorithm to uses the Assorted SIAL CNN model. Figure 1 depicts the model's structure. Convolutions, concatenate, average pooling, and softmax layers are all part of an assorted SAIL convolutional neural network.

4.3.1. Convolution Layer

The convolutional layer is used to extract features. Multi-convolution kernels, parameter sharing, and local perception differentiate this network layer. In contrast to distant pixels, local pixels are tightly interconnected. As additional neurons are linked to each other, the network's complexity will increase. Since each convolutional layer neuron sees only a little piece of the picture, this information is then integrated with other information at a more advanced level. In order to further reduce the network parameters, each layer of neurons has its own set of settings. Neuronal local characteristics may be used to extract features regardless of where they are situated or how many there are. This is because certain statistical aspects of the image are also adapted to other parts of the image.

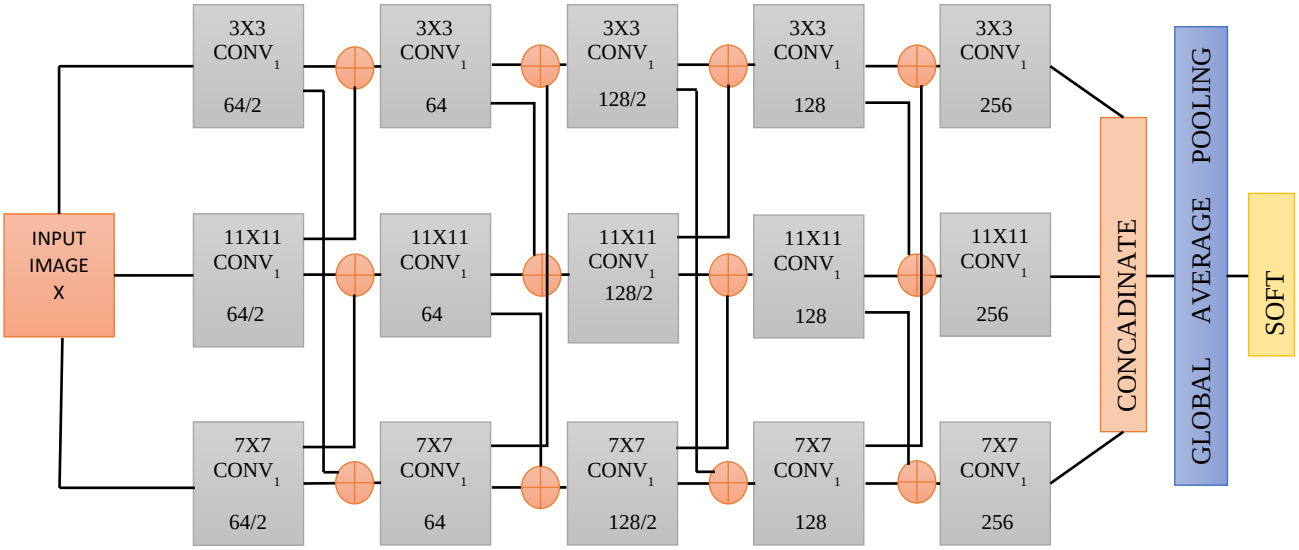

Fig. 1 Schematic representation of the suggested methodology

Figure 1 shows a convolution procedure schematically. Convolution kernels with 3x3, 11x11, and 7x7 pixel sizes will be used to extract multi-scale features. For classification tasks, a convolution kernel size of 3x3 is the norm. Because of the high size of the few lung nodules employed in this proposal, it may not be appropriate for all patients. For this reason, a big filter should be used to transport nodules of this size. To ensure the network's ability and competence, we use a variety of filters at the input. A picture of 32x32 pixels is used in this piece. A q-size convolution kernel and an s-stride filter are used to process an n-dimensional feature map. As a result, the final output maps are,

$$[Out_{map}] = \frac{n-q+s}{s} \cdot \frac{b-q+s}{s} \qquad (5)$$

The number of convolution kernels determines the number of feature maps.

4.3.2. Drop out Layer

Immediately after the convolution layer, there is a dropout layer and a max-pooling layer with a dropout maintenance rate of 0.1 in the odd layer structure. The term "dropout" has been repurposed in an effort to provide uniformity to the educational process. Using this value, the best outcomes may be achieved. Layers may be added element by element since they have comparable dimensions (each layer's output from the one below and the layer above it). An attribute's distinctive potential is boosted by sharing data across all three blocks. It is a good way to increase accuracy. Finally, after the fifth layer, the entire attributes of three levels, $f_1(x)$, $f_2(x)$, and $f_3(x)$, are integrated using the concatenate layer.

$$z_j^{(k+1)} = f\left(\left(l_{ji}\right)z_j^k\right) + a_j \qquad (6)$$

4.3.3. Down-sampling Layer

It is estimated that the term "pooling layer" refers to the layer employed for down-sampling purposes. Averaging statistics from the convolutional layer's feature maps is the function of this layer. Combining the best features and reducing feature size and network parameters may alleviate network overfitting. In addition, the pooling may retain a non-deformational feature (rotation, translation, expansion, etc.). These include mean, max, and stochastic pooling as the most used sampling techniques. Mean sampling is used here, which implies that the average value in each sub-region is utilized as the sample result for each area...

4.3.4. Output Layer

Features derived from convolution layers may be synthesized in a fully connected layer for classification or regression investigations. Global training is performed on the network by reducing its loss function using the features retrieved by the Assorted SIAL CNN.

For multi-classification purposes, Softmax classifiers are an extension of logistic regression models. A training set may be described as follows: let the input feature be $s^{((u))}$ and the sample tag be $a^{((u))}$.

$$A=\{ (s^{(1)},a^{(1)}) (s^{(2)},a^{(2)}) \ldots (s^{(n)},a^{(n)}) \} \qquad (7)$$

Probability $g_\theta(z)$ and the logistic regression cost $h(\theta)$a prediction functions,

$$g_\theta(z) = \frac{1}{\sum_{h=1}^{j} e^{\theta_h^R s^{(u)}}} \begin{bmatrix} e^{\theta_1^R s^{(u)}} \\ e^{\theta_2^R s^{(u)}} \\ \vdots \\ e^{\theta_j^R s^{(u)}} \end{bmatrix} \qquad (8)$$

$$h(\theta) = \frac{1}{n}\left[\sum_{u=1}^{n}\sum_{h=1}^{j} 1\left\{a^{(u)} = h\right\} In \frac{e^{\theta_h^R s^{(u)}}}{\sum_{U=1}^{j} e^{\theta_u^R s^{(u)}}}\right], \qquad (9)$$

In this case, A is the total number of sample tags, and B is the total number of parameters in the network model. Indicative functions, like 1, are defined as follows $1\{\cdot\}$. Depending on whether the value in parentheses is true or false, the function may return one of two potential

outcomes: one or 0. The stochastic gradient descent technique is often used to solve the Softmax cost function (SGD). These two pieces of rules determined the output.

Case 1: Even Block

In this instance, the first level output is integrated with the final level output, or the matching level output is integrated with its prior level output. This method is less expensive than previous procedures since no residual connections exist. Finally, this even block's result may be expressed as follows.

$$O_{e1} = f_1(x_{ie}) + f_L(x_{Le}), i = 1 \quad (10)$$

$$O_{ei} = f_i(x_{ie}) + f_{Li-1}(x_{(i-1)e}), i \in 2,3,\ldots..L \quad (11)$$

Where the inputs to that blocks are x_{1e}, x_{2e}, ... x_{Le}, assuming the even module has L total parallel levels. Their corresponding yields are described as $f_1(x_{1e})$, $f_2(x_{2e})$,.....$f_L(x_{Le})$, respectively. The i stands for the i^{th} level, while O_{ie} stands for the output of the even block's i^{th} level.

Case:2 Odd Block

There are two stages in this process: final and matching. The word "final" refers to this combination of final and matching outputs. The eventual result of this odd block might be shown as,

$$O_{oi} = f_i(x_{io}) + f_{i+1}(x_{(i+1)o}), i \in 1,2,3,\ldots..L-1) \quad (12)$$

$$O_{oL} = f_L(x_{Lo}) + f_1(x_{1o}), i = L \quad (13)$$

The odd module has the input in the form of x_{1o}, x_{2o}, ... x_{Lo}, respectively. Each of their related yields is referred to as $f_1(x_{1o})$, $f_2(x_{2o})$,.....$f_L(x_{Lo})$, and so on. The i stands for the i^{th} level, while O_{io} stands for the odd block's i^{th} level output. Each stage of convolution has a kernel size of k_i. In light of the applications, we may choose the kernel size and the number of layers for each level convolution kernel.

Algorithm: ASAIL CNN

Input: Processed image
Output: Lung nodule classification
Update l_k
Forward Pass:

```
for (1=0;1<K;1++){
    for (n=0;n<N ;n++){
      for (b+0;b<B;b++){
          Sum = bias[1]
       for (j=0;j<J;j++){
            for (a1=0;a1<A1;a1++){
                for (a2=0;a2<A2;a2++){
          Sum+=weight[J][1][a1][a2] × input [j] [n +a1] [b = a2];
        }}}
      output [1] [n] [b] = operative_func(sum)
```

Extract Features $z_j \leftarrow g(y; a)$

Convolve network $z_i^m = \sum_j (l_{ji}^m * y_j^m)$

Compute Drop Layer $z_j^{(k+1)} = f\left((l_{ji}) z_j^k\right) + a_j$

for d_u be the total number of features sample matrix u

for h **in** u **do**

$c_h \leftarrow$ vectorize$_{(h,q)}$
append c_h to d_u
append d_u to d
D_{train}, d_{test}, 1_{train}, 1_{test}, ← break total numbers of features and subset of the train into the labels and subset of test
N ← ASAIL-CNN (d_{train}, 1_{train})
score ← evaluate (u, 1_{test}, N)
return score
Calculate l_{map}
Calculate $l_{map} = l_{map} * Gaussian\ T^j$
Choose Pooling $l_k = max(l_{top}, l_{map})$
Backward pass:
Compute the gradient $\delta k/(\delta l_{jk}^m) = (\delta k/(\delta l_i^m)) * (y_j^m)$
Compute Loss Function $I(\theta) = -\frac{1}{S_{na}} \sum_{S=0}^{S_{na}-1} \sum_{g=0}^{E_{M-1}} \delta_{z^s}^g \ln f_g^{(s)}$
$K_{softmax}(x; l) = -\log softmax_l(x)$
$K_{reg}(s_j, s_j^*) = T(s_j - s_j^*)$
End
End

---

5. Performance Analysis

Assorted SAIL CNN is used to classify binary classification of lung nodules in our experiment, using 70:30 training to test the data ratio. A learning rate of 0.001 was used, together with weight decay parameters of 5*10-4 and a momentum of 0.9, throughout the training stage. Using Adam optimizer is the best option here. It took us 50 epochs to complete the training phase with a batch size of 16. It was used as a loss function. It is also worth noting that there are 256 neurons in the fully connected layer, and the dropout value is set at 0.1.

Moreover, ten-fold cross-validation is used. Tensor flow and tensor layer deep learning structures are employed in our research, which is coded in Python 3.6. We ran our test on a server running Windows 10 and equipped with a Ryzen 7 CPU, 8 GB of RAM, and a 512 GB SSD. The Assorted SAIL CNN model converges in around 12 hours while using the NVIDIA Geforce GTX-1650 GPU for acceleration during model training. A variety of performance criteria are used in a statistical study to assess the number of times the recommended model is effective in diagnosing abnormal lung nodules. In order to evaluate the efficiency of the implementation approaches, we had to standardize critical parameters in all experiments.

Figure 2 depicts the coding process. As shown in the segmentation context, the sigmoid function is a good alternative since it just standardizes the limits and enables extra data to the stream.

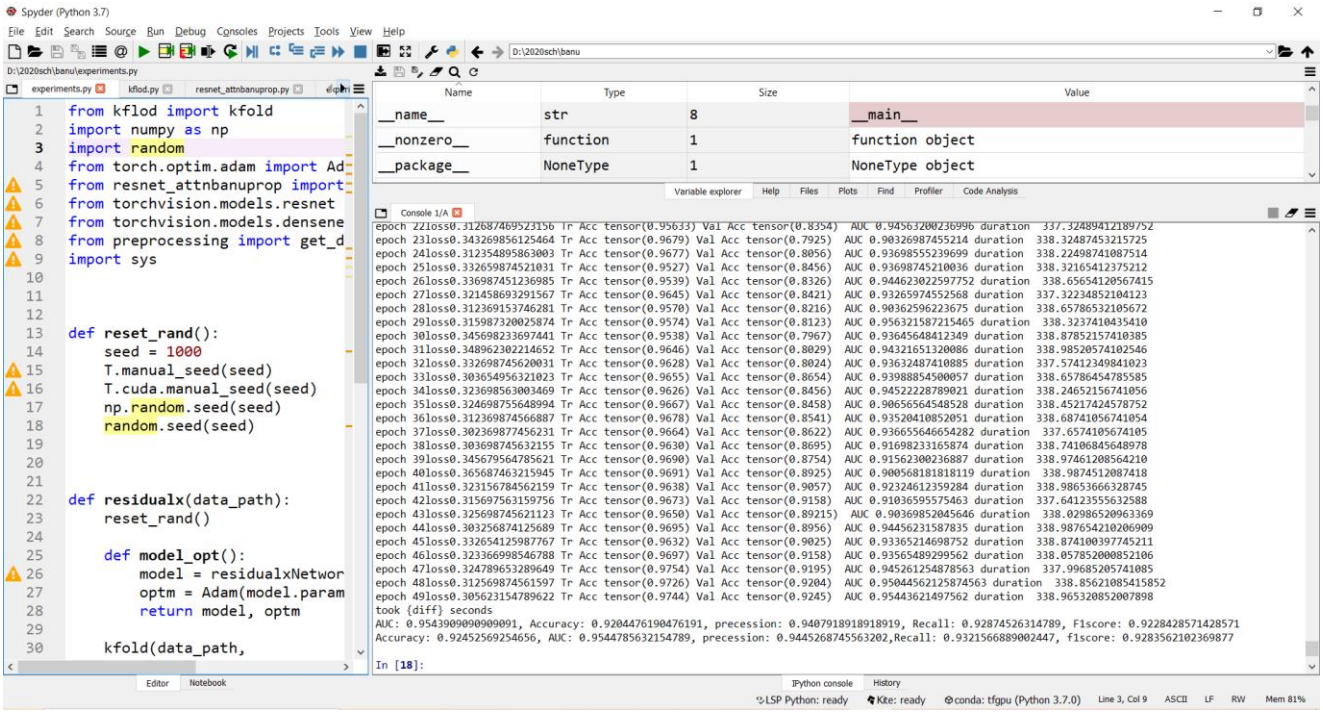

Fig. 2 Process implementation over python

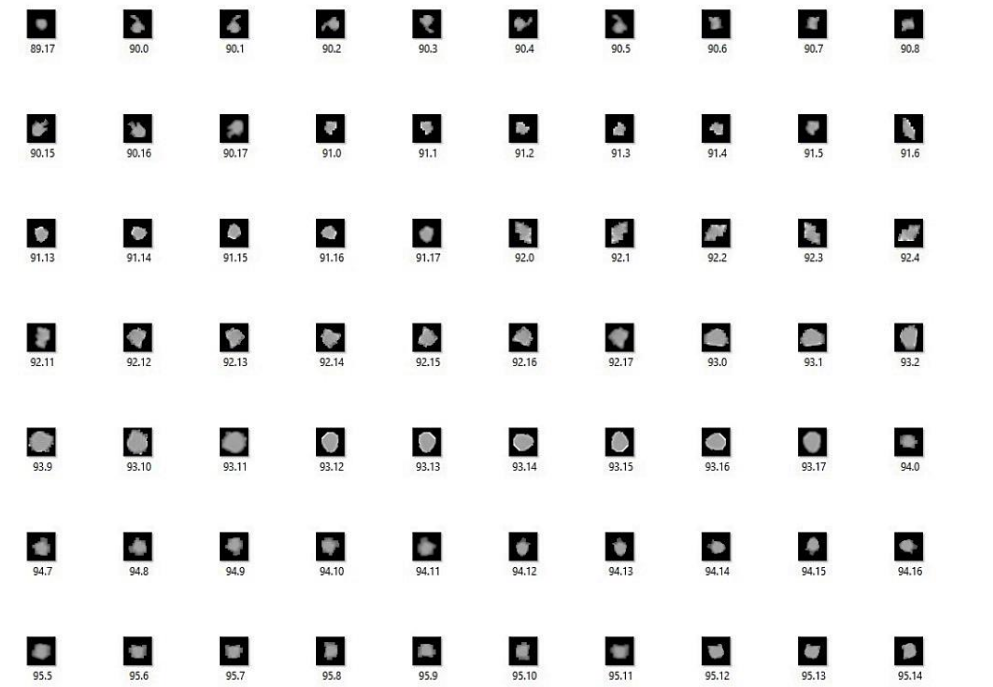

(a)

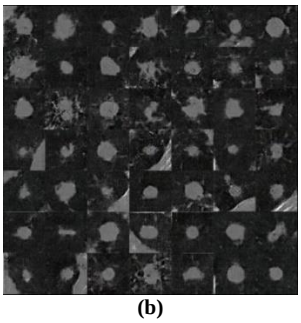

(b)

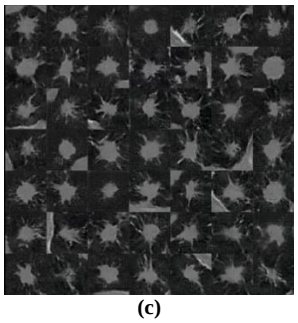

(c)

Fig. 3 Lung nodule classifications

Figure 3(a) shows 2D axial views of lung nodule pictures from the dataset. These illustrations show nodules that are both benign (3 (b)) and malignant (3(c)). Even experienced radiologists have difficulty distinguishing between benign and malignant nodules because of the diagnostic criteria and comparable visual features they share. Our proposed technique makes it possible to distinguish between malignant and benign nodules.

Based on substantial performance measures, the notion is compared to existing algorithms and approaches for identification. The Assorted SAIL CNN was chosen for the anomaly detection task because of its better success rate than other available approaches [21].

5.1. Accuracy

Data quality is the percentage of correct results obtained by the total amount of data points. The accuracy and precision of the recall are shown in percentage.

$$Accuracy\ (A) = (TP + TN)/\ (TP + TN + FP + FN) \quad (14)$$

5.2. Precision

Precision, which represents random errors, is used to quantify algebraic variability.

$$\text{Precision} = [a/(a+d)] \quad (15)$$

5.3. Recall

The percentage of positive information that can be accurately recognized is referred to as the "true optimistic rate," "warning rate," or "probability of identification.".

$$\text{Recall} = [a/(a+d)]\times 100\text{Specificity} \quad (16)$$

Here a represents true positive, and d represents true negative.

5.4. F1 score

Several terms may describe the percentage of positive information that can be correctly recognized.

$$F_1 = \frac{2*Precision*Recall}{Precision+Recall} \quad (17)$$

Table 1. Comparative performance analysis

Techniques	Parameters				
	Accuracy	***AUC***	***Precision***	***Recall***	***f1score***
Resnet50	77.62%	86.82%	80.16%	70.69%	75.13%
AllAtnBig	77.97%	85.89%	81.00%	70.00%	75.10%
Resnet18	78.21%	86.41%	79.00%	75.00%	76.95%
Densenet21	84.57%	92.50%	87.00%	80.00%	83.35%
MLxResnet	89.15%	94.21%	89.55%	90.16%	89.86%
Assorted SAIL CNN	**92.45%**	**95.44%**	**92.45%**	**93.21%**	**92.83%**

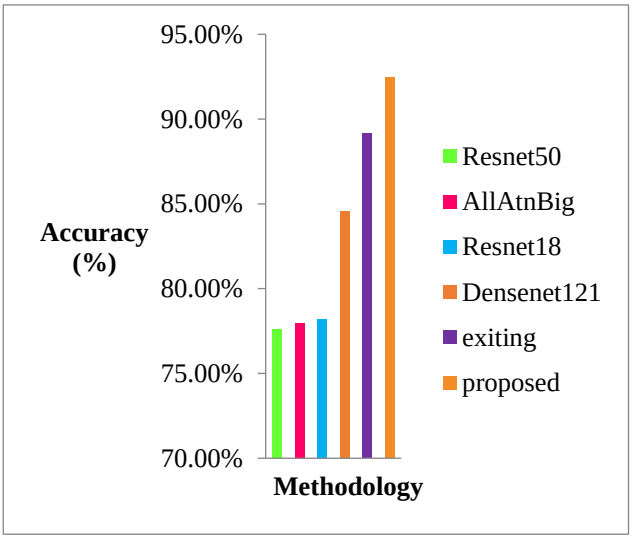

Fig. 4 Methodology Vs. Accuracy

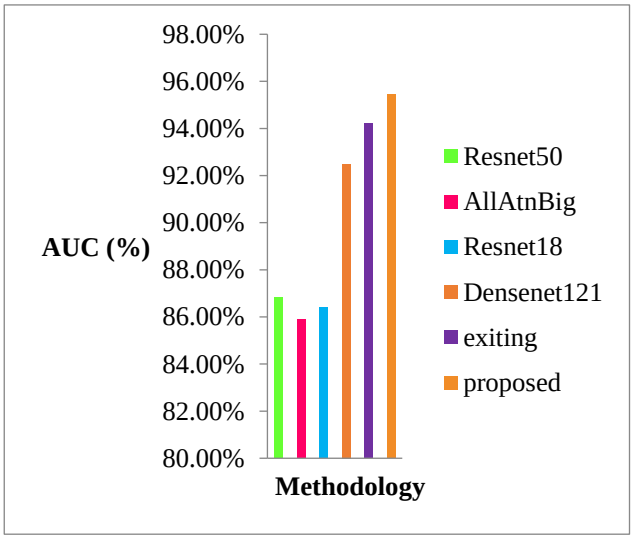

Fig. 5 Methodology Vs. AUC

There is a technique for assessing how many malignant nodules can be correctly classified. It determines how close the results are to the predicted outcome by dividing the total of actual positives and negative outcomes by the number of expected positives and negative outcomes. On the other hand, the proposed method's accuracy (92.45 percent) is higher than that of the current techniques (see Figure 4).

Figure AUC, which is 95.44 %, means that the classifier accurately identified the abnormal class, as shown in Fig.5. The sensitivity/specificity pairs presented at each position on the AUC curve may be used to define decision thresholds. The area under the AUC curve is used to test how successfully a parameter distinguishes between various crops.

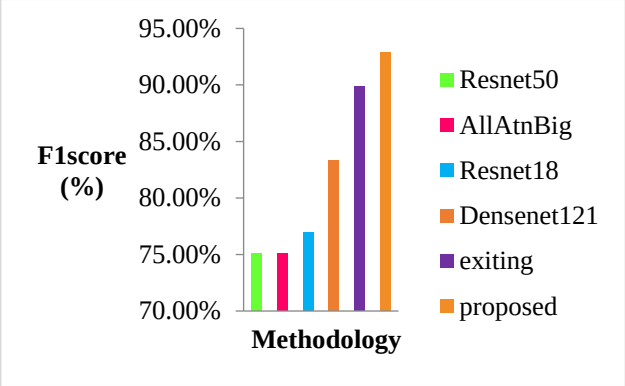

Fig. 6 Methodology Vs. F1Score

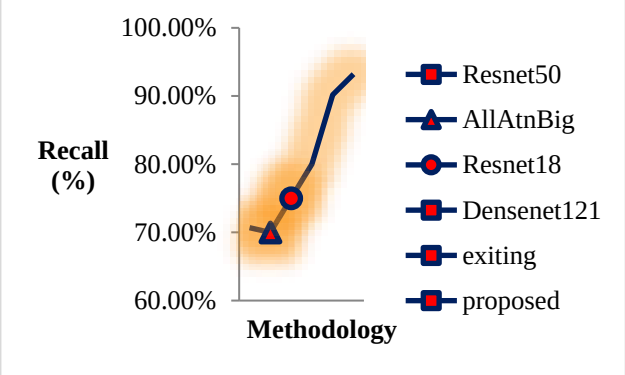

Fig. 7 Methodology Vs. Recall

The F1 score reflects a classifier's ability to correctly identify all nodes that do not have a malignant condition; here, from figure 6, the suggested methods have a high range of the F1 score (92.83%), which was very high when compared to other existing mechanisms.

To correctly determine all nodules with the malignant condition or, if 100% accurate, identify all codes with a faulty condition using HEESO_BA-ZFCNN. Figure 7 shows that the sensitivity of the proposed approaches (93.21%) was quite high compared to other existing mechanisms.

As of figure 8, the precision rate was high (92.45%) for the suggested methodology compared to other existing mechanisms. The result obtained revealed that the suggested methodology outperforms well over malignant nodule classification compared to other existing mechanisms.

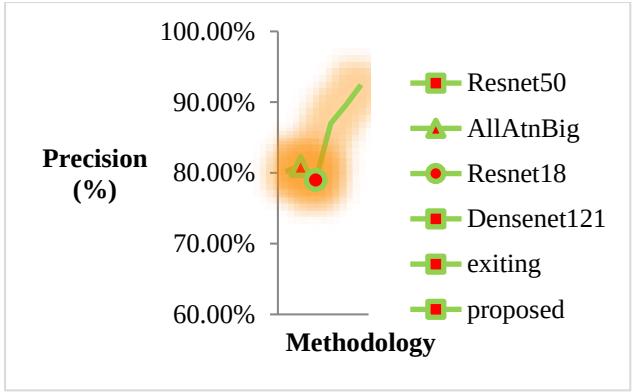

Fig. 8 Methodology Vs. Precision

6. Conclusion

When interpreting chest LIDC-IDRI images, radiologists must distinguish between malignant and benign pulmonary nodules. Inter/intra-observer variability may be exacerbated by this laborious, subjective, time-consuming, and time-consuming manual process. Image processing, classical machine learning, and sophisticated CNN models have been used to develop a variety of computer-aided instruments. However, the classification results derived from nodule lesions cannot be guaranteed in black-box models with little supervision using CNN-based features.

Furthermore, earlier research has demonstrated that greater classification accuracy may be achieved by separating image characteristics taken from the nodule from the area immediately around the nodule. Using disentangled image properties, we describe an ASAIL CNN for classifying benign and malignant lung nodules. To do this, several convolutional pathways are supplied with images of the nodule target and the backdrop. According to our empirical data, CNN-based features have more discriminating power than unsupervised extracted features. The architecture performs better than typical CNNs. As a result of our experiments, we gathered and identified the nodule's complicated attributes with a broad range of prediction accuracy (92.45 percent). In the future, nodules of size between 3 -30 mm were considered. It provides useful information for determining whether or not a nodule is present. Other feature reduction and selection methods might be used to find the traits that will be used to characterize the lung tumor.

References

[1] Y. Su, D. Li, and X. Chen, "Lung Nodule Detection Based on Faster R-CNN Framework," *Computer Methods and Programs in Biomedicine*, vol. 200, 2021. Crossref, https://doi.org/10.1016/j.cmpb.2020.105866

[2] D. Gu, G. Liu, and Z. Xue, "On the Performance of Lung Nodule Detection, Segmentation and Classification," *Computerized Medical Imaging and Graphics*, vol. 89, 2021. Crossref, https://doi.org/10.1016/j.compmedimag.2021.101886

[3] Xiangde Luo, Tao Song, Guotai Wang, Jieneng Chen, Yinan Chen, Kang Li, Dimitris N. Metaxas, and Shaoting Zhang, "SCPM-Net: An Anchor-Free 3d Lung Nodule Detection Network Using Sphere Representation and Center Points Matching," *Medical Image Analysis*, vol. 75, 2022. Crossref, https://doi.org/10.1016/j.media.2021.102287

[4] Z. Ali, A. Irtaza, and M. Maqsood, "An Efficient U-Net Framework for Lung Nodule Detection Using Densely Connected Dilated Convolutions," *The Journal of Supercomputing*, vol. 78, pp. 1602-1623, 2022. Crossref, https://doi.org/10.1007/s11227-021-03845-x

[5] Talha Meraj, Hafiz Tayyab Rauf, Saliha Zahoor, Arslan Hassan, M. IkramUllah Lali, Liaqat Ali, Syed Ahmad Chan Bukhari, and Umar Shoaib, "Lung Nodules Detection Using Semantic Segmentation and Classification with Optimal Features," *Neural Computing and Applications*, vol. 33, pp. 10737-10750, 2021. Crossref, https://doi.org/10.1007/s00521-020-04870-2

[6] Y. Bai, D. Li, Q. Duan, and X. Chen, "Analysis of High-Resolution Reconstruction of Medical Images Based on Deep Convolutional Neural Networks in Lung Cancer Diagnostics," *Computer Methods and Programs in Biomedicine*, vol. 217, 2022. Crossref, https://doi.org/10.1016/j.cmpb.2021.106592

[7] B. Yin, M. Sun, J. Zhang, W. Liu, C. Liu, and Z. Wang, "AFA: Adversarial Frequency Alignment for Domain Generalized Lung Nodule Detection," *Neural Computing and Applications*, vol. 34, pp. 8039–8050, 2022. Crossref, https://doi.org/10.1007/s00521-022-06928-9

[8] F.Y. Lin, Y.C. Chang, H.Y. Huang, C.C. Li, Y.C. Chen, and C.M. Chen, "A Radiomics Approach for Lung Nodule Detection in Thoracic CT Images Based on the Dynamic Patterns of Morphological Variation," *European Radiology*, pp. 1-11, 2022. Crossref, https://doi.org/10.1007/s00330-021-08456-x

[9] R. Manickavasagam, S. Selvan, and M. Selvan, "Cad System for Lung Nodule Detection using Deep Learning With Cnn," *Medical & Biological Engineering & Computing*, vol. 60, no. 1, pp. 221-228, 2022. Crossref, https://doi.org/10.1007/s11517-021-02462-3

[10] S. Dodia, A. Basava, and M. Padukudru Anand, "A Novel Receptive Field-Regularized V-Net and Nodule Classification Network for Lung Nodule Detection," *International Journal of Imaging Systems and Technology*, pp. 88-101, 2022. Crossref, https://doi.org/10.1002/ima.22636

[11] A. Bilal, G. Sun, Y. Li, S. Mazhar, and J. Latif, "Lung Nodules Detection Using Grey Wolf Optimization by Weighted Filters and Classification Using CNN," *Journal of the Chinese Institute of Engineers*, vol. 45, no. 2, pp. 175-186, 2021. Crossref, https://doi.org/10.1080/02533839.2021.2012525

[12] N. S. El-Askary, M. A.-M. Salem, and M. I. Roushdy, "Features Processing for Random Forest Optimization in Lung Nodule Localization," *Expert Systems with Applications*, vol. 193, 2022. Crossref, https://doi.org/10.1016/j.eswa.2021.116489

[13] N. A. Pande and D. Bhoyar, "A Comprehensive Review of Lung Nodule Identification Using an Effective Computer-Aided Diagnosis (CAD) System," *In 2022 4th International Conference on Smart Systems and Inventive Technology (ICSSIT)*, pp. 1254-1257, 2022. Crossref, https://doi.org/10.1109/ICSSIT53264.2022.9716327

[14] A. Halder, S. Chatterjee, and D. Dey, "Adaptive Morphology Aided 2-Pathway Convolutional Neural Network for Lung Nodule Classification," *Biomedical Signal Processing and Control*, vol. 72, 2022. Crossref, https://doi.org/10.1016/j.bspc.2021.103347

[15] M. Al-Shabi, K. Shak, and M. Tan, "Procan: Progressive, Growing Channel Attentive Non-Local Network for Lung Nodule Classification," *Pattern Recognition*, vol. 122, 2022. Crossref, https://doi.org/10.1016/j.patcog.2021.108309

[16] N. Ali and J. Yadav, "Computer-Aided Detection and Diagnosis of Lung Nodules Using CT Scan Images: An Analytical Review," *In Proceedings of Second Doctoral Symposium on Computational Intelligence*, vol. 1374, 2022. Crossref, https://doi.org/10.1007/978-981-16-3346-1_44

[17] He Ma, Huimin Guo, Mingfang Zhao, Shouliang Qi, Heming Li, Yumeng Tian, Zhi Li, Guanjing Zhang, Yudong Yao, and Wei Qian, "Automatic Pulmonary Ground-Glass Opacity Nodules Detection and Classification Based on 3d Neural Network," *Medical Physics*, vol. 49, no. 4, pp. 2555-2569, 2022. Crossref, https://doi.org/10.1002/mp.15501

[18] I. D. Kawathekar and A. S. Areeckal, "Performance Analysis of Texture Characterization Techniques for Lung Nodule Classification," *In Journal of Physics: Conference Series*, vol. 2161, 2022. Crossref, https://doi.org/10.1088/1742-6596/2161/1/012045

[19] V. Kumar and B. Bakariya, "Detection of Lung Malignancy Using Squeezenet-Fc Deep Learning Classification Technique," *In Proceedings of the International Conference on Paradigms of Communication, Computing and Data Sciences*, pp. 683-699, 2022. Crossref, https://doi.org/10.1007/978-981-16-5747-4_5

[20] Taeho Ha, Wooil Kim, Jaehyung Cha, Young Hen Lee, Hyung Suk Seo, So Young Park, Nan Hee Kim, Sung Ho Hwang, Hwan Seok Yong, Yu-Whan Oh, Eun-Young Kang, and Cherry Kim, "Differentiating Pulmonary Metastasis From Benign Lung Nodules in Thyroid Cancer Patients Using Dual-Energy CT Parameters," *European Radiology*, vol. 32, pp. 1902-1911, 2022. Crossref, https://doi.org/10.1007/s00330-021-08278-x

[21] M. Al-Shabi, B. L. Lan, W. Y. Chan, K.-H. Ng and M. Tan, "Lung Nodule Classification Using Deep Local–Global Networks," *International Journal of Computer Assisted Radiology and Surgery*, vol. 14, no. 10, pp. 1815-1819, 2019. Crossref, https://doi.org/10.1007/s11548-019-01981-7

[22] M.M.Adem, and A.Jagtap, "A Survey on Early Detection of Lung Cancer by Gene Expression Profiles using Data Mining Techniques," *International Journal of Engineering Trends and Technology*, vol.55, pp.21-24, 2018. Crossref, https://doi.org/10.14445/22315381/IJETT-V55P205.

[23] M.M.A.Priya, and S.J.Jawhar, "Lung Disease Identification and Segmentation in Medical Images," *International Journal of Engineering Trends and Technology*, vol. 67, no. 8, pp. 87-91, 2019. Crossref, https://doi.org/10.14445/22315381/IJETT-V67I8P215

[24] A.Bhandary, G.A.Prabhu, M.Basthikodi, and K.M.Chaitra, "Early Diagnosis of Lung Cancer Using Computer-Aided Detection via Lung Segmentation Approach," *International Journal of Engineering Trends and Technology*, vol. 69, no. 5, pp. 85-93, 2021. Crossref, https://doi.org/10.14445/22315381/IJETT-V69I5P213

[25] S. Farjana Farvin, and S. Krishna Mohan, "A Comparative Study on Lung Cancer Detection using Deep Learning Algorithms," *SSRG International Journal of Computer Science and Engineering*, vol. 9, no. 5, pp. 1-4, 2022.
Crossref, https://doi.org/10.14445/23488387/IJCSE-V9I5P101

[26] Rabiya Banu. A, and Kannan. R, "Quantitative and Qualitative Analysis for Lung Nodule Segmentation," *SSRG International Journal of Electronics and Communication Engineering*, vol. 6, no. 5, pp. 16-21, 2019.
Crossref, https://doi.org/10.14445/23488549/IJECE-V6I5P104